

## Chapter 3 – Radiation damage effects

### 3.1 The radiation damage mechanism

This chapter presents the damage in silicon detectors inflicted by the radiation and the consequences for the operation of the detectors. The radiation damage mechanism in silicon detectors can be divided in two classes: surface damage and bulk damage.

#### Surface damage

The passage of an ionising radiation in silicon detectors creates e-h pairs that are collected by the electric field at the electrodes and form the signal. In the undepleted bulk of the semiconductor, where there is no electric field, the high carrier density allows the deposited charge carriers to recombine. Therefore, the semiconductor does not show permanent traces of the passage of a charged particle that loses energy by ionisation. On the contrary, the passage of an ionising radiation in the oxide causes the built up of trapped charge in the oxide layers of the detector. The e-h pairs created in the oxide either recombine or move in the oxide electric field: the electrons towards the SiO<sub>2</sub>-Si interface, the holes towards the metallic contact. The higher mobile electrons escaped from the recombination are injected into the silicon bulk, in a typical time of  $\approx 100$  ps. The less mobile holes can be trapped at the SiO<sub>2</sub>-Si interface. This trapping results in an increase of the oxide positive charge [3.1], and therefore in a degradation of the oxide quality. In addition to the trapped charge, the ionising radiation also produces new energy levels in the band gap at the SiO<sub>2</sub>-Si interface. These levels can be occupied by electrons or holes, depending on the position of the Fermi level at the interface [3.2, 3.3] and the corresponding charge can be added or subtracted to the oxide charge. The effects of the radiation on the oxide and the surface damage are dependent on the specific detector design and are beyond the scope of this thesis.

#### Bulk damage

The bulk damage is caused by the non-ionising energy loss (NIEL) interactions of a primary

particle with mass  $m_p$  and energy  $E_p$  with a lattice silicon atom with mass  $M_{Si}$ . The energy transferred in the interaction is, in the non-relativistic case:

$$\Delta E = 4 \frac{m_p M_{Si}}{(m_p + M_{Si})^2} \sin^2\left(\frac{\vartheta}{2}\right) \cdot E_p \quad (3.1)$$

where  $\vartheta$  is the scattering angle. Displacement damage occurs whether the energy transferred to the silicon atom is sufficient to remove it from the crystal lattice. The atom is then called *primary knock-on atom* (PKA). The minimum threshold energy for the displacement is  $\approx 15$  eV [3.5]. The vacancy-interstitial (V-I) silicon created is called a *Frankel pair*. The minimum energy for particles like neutrons or protons, with mass  $\approx 1$  u, required to create a Frankel pair is  $\approx 110$  eV. The same threshold energy for electrons is  $\approx 260$  keV. The energy of the particle used for the irradiation studies reported in the present work is several orders of magnitude higher than the threshold level, as it will be in the background radiation in the inner detectors of LHC.

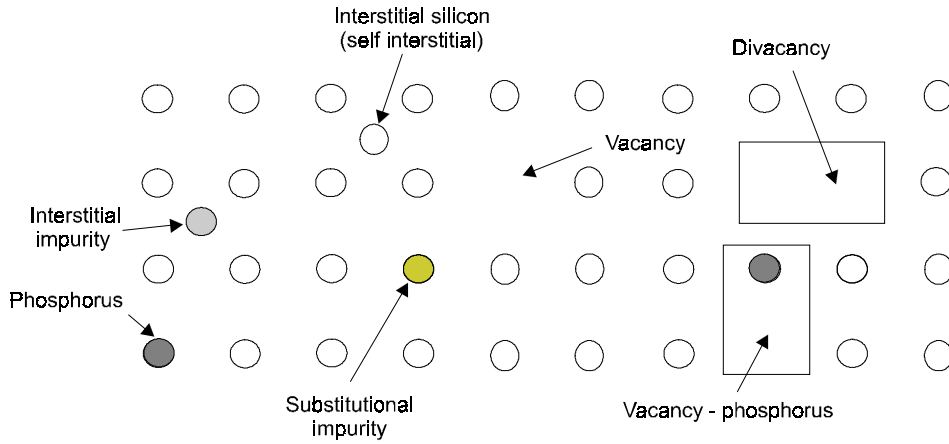


Fig. 3.1 *Diagram of some defects in the n-type silicon crystal lattice due to point defect Complexes.*

The recoil energy of the PKAs can be up to 130 keV and therefore they can remove other atoms from the crystal lattice, giving rise to a PKA cascade. It has been estimated [3.5] that  $\approx 50\%$  of the energy of the recoil atom is deposited via ionisation and the displacement dominates when the recoil atom loses its final 5-10 keV. The fraction of energy going to the non-ionising interaction is described by the Lindhard partition function. The cascade results in the formation of two or three terminal clusters of  $\approx 50$  Å linear dimension with high concentration of Frankel defects [3.6]. About 90% of the vacancies recombine with interstitials, leaving no net damage in the crystal. Some vacancies can form stable divacancy

(or multi-vacancy) defect complexes and the remaining vacancies and interstitials diffuse through the crystal and react with other defects or impurity atoms always present in the silicon crystal (O, C, P, B...) to form stable complexes. The introduction rate of vacancies (V) and divacancies (V<sub>2</sub>) have been determined to be  $\eta_V = 2.1 \pm 0.5 \text{ cm}^{-1}$  and  $\eta_{V_2} = 4.7 \pm 0.4 \text{ cm}^{-1}$  for 1 MeV neutron irradiation [3.6]. Figure 3.1 shows an example of the final damage due to aggregation of point defects (V<sub>2</sub>, VP) and Fig. 3.2 shows the clusters resulting from the irradiation with high-energy hadrons.

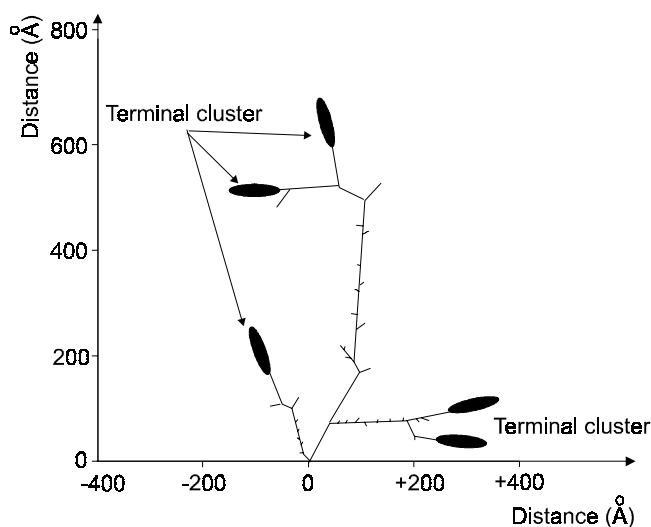


Fig. 3.2 *Picture of a typical recoil-atom track with formation of final highly damaged regions (clusters) as a consequence of hadron irradiation [3.2]*

Clusters are thought to be responsible for the significant differences between the damage created by light particles (photons and low energy electrons) and heavy particles. Electrons with energy up to few hundred keV can displace only one or two silicon atoms from their lattice sites. The generation of V<sub>2</sub> (or higher vacancy complexes, V<sub>3</sub>, V<sub>4</sub>...) states is therefore limited and most defects are of the vacancy-impurity type. The damage due to light particles has been studied by electron and gamma irradiation [3.8, 3.9, 3.10] (e.g. <sup>60</sup>Co photons with energy 1.17 and 1.33MeV. The scattered Compton electrons have energies of a few hundred keV).

The density of vacancies in clusters leads to the enhanced formation of divacancies. The ratio between the introduction rate of vacancies to divacancies is  $\approx 100$  times greater for heavy particle damage than for gamma-ray damage. There is evidence that the V<sub>2</sub> defects are formed

by the vacancies created in close proximity, so in the same cluster, rather than in clusters related to different displacement events. [3.11, 3.12].

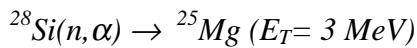
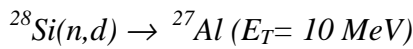
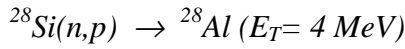
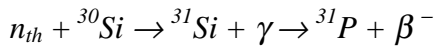
Another mechanism of damage in silicon is through nuclear reaction of silicon nuclei with the impinging radiation. The natural abundance of  $^{28}\text{Si}$  silicon isotope is 92.2 %, 4.7% of  $^{29}\text{Si}$  and 3.09% of  $^{30}\text{Si}$ . Various nuclear reactions can take place with the different Si isotopes and the introduction rate of a specific nucleus can be expressed by

$$\eta = f \cdot \sigma(E) \cdot 8/a^3 \quad (3.2)$$

where  $a = 5.43 \text{ \AA}$ ,  $f$  is the fraction of natural abundance of Si isotope and  $\sigma(E)$  is the cross section of the specific reaction. If the incident radiation is not mono-energetic, the introduction rate will be expressed by integration over the energy spectrum

$$\eta = \frac{\int_0^{\infty} d(E) \varphi(E) f \cdot \sigma(E) \frac{8}{a^3}}{\int_0^{\infty} d(E) \varphi(E)} \quad (3.3)$$

where  $\varphi(E)$  is the differential particle flux spectrum for the normalisation ( $\text{MeV}^{-1}$ ). The resulting high-energy fragments could be involved in damage processes. Possible nuclear reactions with silicon isotopes are



where  $n_{th}$  is a thermal neutron and  $E_T$  is the threshold energy of the specific reaction. The first reaction is used for the NTD silicon doping [3.13]. The produced Al and Mg nuclei introduce shallow acceptor energy levels if they are in substitutional sites or donors if they are in interstitial sites [2.1]. Anyway, the introduction rate of all these species does not seem to be that important compared to the introduction rate of defects correlated with the displacement damage.

To describe globally the radiation effect on silicon, it has been assumed that the damage is proportional to the energy deposited into the displacement interactions (NIEL hypothesis)[3.14]. The displacement damage cross section  $D(E_p)$  expresses the relative displacement efficacy of an impinging particle  $p$  with energy  $E_p$ , taking into account the

various type of interactions between the particle and the silicon atom. The displacement damage cross section is defined by [3.15]:

$$D(E_p) = \sum_i \sigma_i(E_p) \int_{E_{Rmin}}^{E_{Rmax}} dE_R f_i(E_p, E_R) P(E_R) \quad (3.4)$$

where the sum is over all the possible interactions. The function  $f_i$  describes the distribution of the recoil atom with energy  $E_R$  and  $P(E_R)$  is the Lindhard partition function of the energy loss in non-ionising processes by a recoiling nucleus of energy  $E_R$ . The lower bound of the integral corresponds to the minimum energy required to displace a silicon atom from the lattice and the upper limit is determined by the maximum energy transferred.

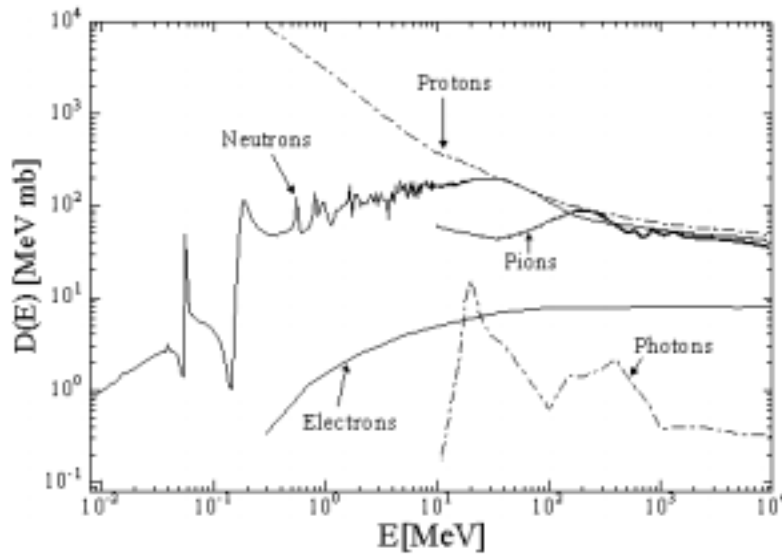


Fig. 3.3 Displacement damage cross section as a function of energy for various particle in silicon [3.16].

The total displacement damage energy per volume, deposited in a crystal undergoing irradiation is

$$T_{dam} = N \cdot t_{exp} \int_0^{\infty} dE_p \varphi(E_p) D(E_p) \quad (3.5)$$

where  $N$  is the number of silicon atoms per unit of volume,  $\varphi(E_p)$  is the differential particle flux spectrum and  $t_{exp}$  is the exposure time. Fig. 3.3 [3.16] shows the displacement damage cross section for various particles as a function of their energy. It is possible to relate the displacement damage caused by the integrated flux of the particle spectrum in eq. 3.4 to a reference particle. Usually the reference particle is 1 MeV neutron. The *hardness factor*,  $k$ ,

used to express the radiation damage in term of the 1 MeV neutron equivalent fluence, is defined by:

$$k = \frac{1}{D_n(1MeV)} \frac{\int_{E_{min}}^{E_{max}} dE_p \varphi(E_p) D(E_p)}{\int_{E_{min}}^{E_{max}} dE_p \varphi(E_p)} \quad (3.6)$$

The  $k$  factor for 1 MeV neutron is assumed to be one and the corresponding value of  $D(1MeV)$  is 95 MeV mb. The equivalent fluence for an arbitrary radiation is then

$$\Phi_{eq} = k\Phi_{meas} = k \int_{E_{min}}^{E_{max}} dE_p \varphi(E_p) \quad (3.7)$$

Table 3.1 summarises the hardness factor for the radiation sources used in the present work.

Source name	Particle type	Hardness factor
CERN-PST7	Monochromatic protons, 24 GeV/c	0.5
Ljubljana Triga nuclear reactor	Neutron fission spectrum	0.75

Table 3.1 *Hardness factor for the normalisation to the 1MeV neutron fluence for the two facilities used for the irradiation.*

### 3.2 Changes in detector properties

The final radiation damage is due to the thermally stable defects formed by the reaction of primary defects (V, interstitial) with other defects or atomic impurities. Some of the possible reaction have been identified and are reported in Table 3.2. Some of the stable complexes are electrically active, therefore the changes of the electrical properties of detectors are correlated with the electrical activity of the stable damage. Several defects have been identified by means of different measurement techniques, such as electron paramagnetic resonance (EPR), photoluminescence, current or capacitance deep level transient spectroscopy (I-DLTS, C-DLTS), thermally stimulated current (TSC). Table 3.3 lists some of the identified defects, their charge states and their associated energy levels in the band gap. Most of these energy levels

situate in the deep region of the silicon band gap, close to the middle. Figure 2.5 illustrates the possible processes occurring at the intermediate levels in the band gap. These are correlated with the changes in the electrical properties of detectors.

The generation process (Fig. 2.5(a)) is the thermal creation of an e-h pair when an electron is excited from the valence band to the conduction band, through an intermediate defect level. It can be regarded as the simultaneous emission of a hole and an electron into the valence and the conduction band, respectively. This results in an increase of the leakage current in the reverse bias operations. Recombination (Fig. 2.5(b)) happens when an electron from the conduction band combines with a hole in the valence band at the level corresponding to the defect. Recombination influences the forward current.

The trapping (Fig. 2.5(c)) is the capture of a carrier from the conduction band to the trap energy level, followed by the emission of the carrier itself back to the conduction band. This process affects the collection time of the charge generated by ionisation in the detector and the carrier mobility.

The trapping effect can be also quasi-permanent, depending on the position of the level in the band gap (Fig. 2.5(d)). In that case, the defect changes its charge state and contributes to the space charge in the depleted volume of the detector, acting as a compensation centre.

Models that associate the properties of the deep levels to radiation damage have been proposed. The idea is to explain the changes in the electrical behaviour using a limited amount of reactions between radiation induced defects and impurities. The identification of the stable defects responsible for these changes and the knowledge of the kinetics of their formation should suggest the species and the concentrations of the impurities that are suitable for improvement of the radiation tolerance of silicon. The aim is to induce alternative reactions to form electrically inactive complexes and reduce the effects of the radiation damage.

The radiation damage effects of interest for high-energy physics applications concern the modification of the electrical properties of silicon detectors. The requirements to the silicon detectors are high signal to noise ratio and low heating dissipation (low leakage currents) during the operation time of the experiment. The degradation of the electrical characteristic inflicted by the radiation makes more difficult the fulfilment of the basic requirements to the detectors.

This chapter describes the changes induced by the radiation to the electrical performance of

silicon detectors.

I reactions	V reactions	C <sub>i</sub> reactions
I + C <sub>s</sub> → C <sub>i</sub>	V + V → V <sub>2</sub>	C <sub>i</sub> + C <sub>s</sub> → CC
I + CC → CCI	V + V <sub>2</sub> → V <sub>3</sub>	C <sub>i</sub> + O → CO
I + CCI → CCII	V + O → VO	
I + CO → COI	V + VO → V <sub>2</sub> O	
I + COI → COII	V + P → VP	
I + VO → O		
I + CV <sub>2</sub> → V		
I + VP → P		

Table 3.2 A few defect reactions in silicon. The subscript *i* stands for interstitial, *s* for substitutional, *I* for Si interstitial, *V* for vacancy, *C* for carbon, *O* for Oxygen and *P* for phosphorus.

Defect	Energy level	Defect type
VO	E <sub>C</sub> - 0.17	acceptor
V <sub>2</sub> O	E <sub>C</sub> - 0.50	acceptor
V <sub>2</sub>	E <sub>C</sub> - 0.23	acceptor
	E <sub>C</sub> - 0.42	acceptor
	E <sub>V</sub> + 0.25	donor
VP	E <sub>C</sub> - 0.45	acceptor
CC	E <sub>C</sub> - 0.17	acceptor
CO	E <sub>V</sub> + 0.36	donor

Table 3.3 Identified defect states with their energy levels in eV.

### 3.2.1 Reverse Current

It has been noticed (§ 2.2) that the leakage current in a reverse biased junction has a bulk component depending on the concentration of generation centres.

It is observed experimentally that the leakage current of a reverse biased detector increases linearly with fluence. The dependence of the current per unit volume ( $I_{vol}$ ) on the damaging particle fluence can be written as it follows:

$$\Delta I_{vol} = I_{vol}(\Phi) - I_{vol}(\Phi = 0) = \alpha \cdot \Phi \quad (3.8)$$

where the constant  $\alpha$  is called the *reverse current damage factor*. The proportionality to the fluence implies that the increase of the current is due to the linear introduction of active generation centres, which dominate the reverse current (§2.2). In this case, the current is proportional to the depleted volume, then to the square root of bias up to  $V_{FD}$  and saturates for bias voltages above full depletion (Fig. 3.4).  $I_{vol}$  can be defined as the reverse current at full diode depletion.

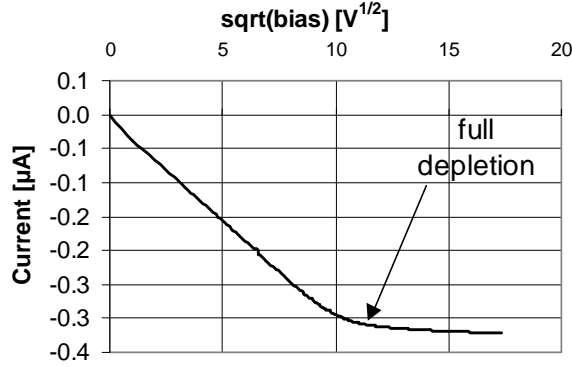


Fig. 3.4 The reverse current characteristic as a function of the square root of the reverse bias. The reverse current is proportional to the depleted volume until full depletion.

The leakage current is strongly influenced by the temperature. The results will be presented normalised to the room-temperature (20 °C). The temperature dependence of the leakage current has been extensively studied [3.17-3.20] and the data are found to fit the form:

$$I \propto T^2 \exp\left(-\frac{E_A}{k_B(T + 273.2)}\right) \quad (3.9)$$

where  $E_A$  is the activation energy and  $T$  the temperature in Celsius. The values of  $E_A$  found by different workers are ranging from 0.6 to 0.7 eV [3.21, 3.22]. The value accepted in the present work is  $E_A = 0.62$  eV. The correction of the reverse current data are performed according to:

$$\frac{I_{20}}{I_T} = \left(\frac{293.2}{273.2+T}\right)^2 \exp\left[\frac{0.62}{k_B}\left(\frac{1}{273.2+T} - \frac{1}{293.2}\right)\right] \quad (3.10).$$

In order to compare the damage due to different particles with different energies, the fluence value have to take into account the NIEL radiation damage factor. On the other hand, the linearity of  $\alpha$  allows the experimental determination of the NIEL damage factor of different particles with different energy spectra, by irradiating identical detectors with these particles.

### Annealing correction of the leakage current

After irradiation, the reverse current evolves as function of time and temperature. Fig.3.5 shows the changes of the radiation damage constant,  $\alpha$ , for diodes irradiated at different temperatures with 24GeV/c protons and then stored at these temperatures [3.20].

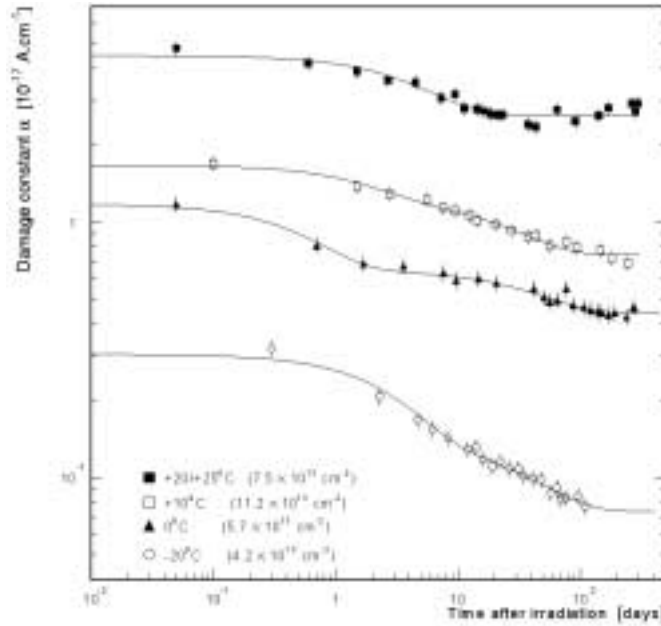


Fig.3.5 Radiation damage constant,  $\alpha$ , as a function of time after irradiation for silicon detectors irradiated and stored at various temperatures [3.20].

The reverse current anneals with a series of time constants,  $\tau_i$ , and can be parameterised as it follows

$$\Delta I_{vol}(t, \Phi) = \Delta I_{vol}(0, \Phi) \sum_i a_i \exp\left(-\frac{t}{\tau_i}\right), \quad \sum_i a_i \equiv 1 \quad (3.11)$$

where  $\Delta I_{vol}(t, \Phi)$  is the change of the reverse current as a function of the time after irradiation and  $\Delta I_{vol}(0, \Phi)$  is the value of the reverse current at the end of the irradiation up to the fluence  $\Phi$ . Here the irradiation time needed to accumulate the fluence  $\Phi$  is neglected. The parameters  $a_i$ 's weigh the individual contributions to the reverse current. Two sets of parameters have been established in [3.23] to fit the reverse current annealing data. They are reported in Table 3.4 for non-inverted and inverted n-type silicon detectors (see below the definition of type inversion). These sets of parameters are valid for detectors made of standard silicon. The microscopic explanation for the annealing behaviour is still not satisfactory and the correlation between the identified radiation induced defects and the annealing of the leakage current is not available. It is therefore possible that the annealing characteristic of detectors manufactured by non-standard silicon is different. Nevertheless, this description of the leakage current annealing is successful and describes well the experimental data obtained so far.

It is expected, from this parameterisation, that a fraction of the radiation-induced current does not anneal. It is then possible to define the value of the radiation damage constant after infinite time annealing at room temperature ( $T_{RT}$ ) as it follows:

$$\alpha_{\infty} = \frac{\Delta I_{Vol}(\Phi, \infty, T_{RT})}{\Phi} \quad (3.12)$$

<b>Inverted</b>		<b>Not inverted</b>	
$\tau_i$ [min.]	$a_i$	$\tau_i$ [min.]	$a_i$
13.5	0.197	17.8	0.156
84.3	0.3	119	0.116
1550	0.121	1090	0.131
8740	0.139	14800	0.201
$\infty$	0.243	89200	0.093
		$\infty$	0.303

Table 3.4 *Fitting parameters for the annealing at room temperature of the reverse current of detectors made from standard silicon.*

The assumption of the stabilisation of the reverse current is not justified on a physical basis. The correlation between the time constants and the evolution with time of the defects has not been established yet. Recent results report values of annealing time constant of irradiated silicon as long as  $\approx 860 \pm 200$  days for an annealing temperature of  $\approx 45^\circ\text{C}$  [3.31]. This implies the existence of a very long component of the annealing at room temperature of the leakage current, showing that  $\alpha_{\infty}$  cannot be calculated on the base of the measurement of the current after  $\approx 10$  days. Anyway, the parameterisation proposed in Table 3.4 reproduces well the experimental data over the time scale of interest (corresponding to a few years at room temperature). The value of  $\alpha_{\infty}$  corresponds to an almost stable value of the current during a few years. With this assumption, the changes of the leakage current of silicon detectors made of different starting materials can be compared using the value of the radiation damage constant immediately at the end of the irradiation ( $\alpha_0$ ) or using  $\alpha_{\infty}$  as defined above. Equation 3.11, with the parameters reported in Table 3.4, is used to calculate  $\alpha_0$  from the I-V data after irradiation.

The calculation is performed taking into account the irradiation time needed to accumulate the required fluence and the time elapsed after the end of the irradiation. The value of the current is the value estimated at the end of the irradiation and as the irradiation would be performed in a negligible time.

### 3.2.2 Effective doping concentration

Many workers [3.17-3.26] have experimentally found that  $N_{eff}$  changes as a function of the fluence,  $\phi$ . The  $N_{eff}$  behaviour of n-type silicon can be fitted to the empirical function [3.27]

$$N_{eff} = |N_D e^{-c\phi} - N_A - \beta\phi| \quad (3.13)$$

where  $N_D$  is the initial donor concentration,  $N_A$  is the initial acceptor concentration (the compensation level),  $c$  describes the removal rate of initial donors and  $\beta$  is the parameter accounting for the introduction of acceptor-like defects. The radiation induced acceptor defects are found to be dominant: it has actually been measured that the doping concentration of initial n-type silicon diodes decreases progressively as a function of the received fluence until the diodes invert to effectively p-type. After conductivity type inversion, the p-type  $N_{eff}$  increases linearly with fluence.

The parameterisation of the radiation induced behaviour of n-type silicon diodes implies donor removal and linear introduction rate of acceptor-like defects. Figure 3.6 shows an example of  $N_{eff}(V_{FD})$  versus pion fluence as reported in [3.28], and the results of fit according to eq. 3.13.

For n-type silicon detectors, the conductivity type inversion fluence depends on the initial resistivity  $\rho$ , which is related to the effective doping concentration before irradiation  $N_{eff}(0)$  by:

$$\rho \approx \frac{1}{\mu q N_{eff}(0)}. \quad (3.14)$$

The dependence of the type inversion fluence ( $\phi_{inv}$ ) on  $N_{eff}(0)$  for diodes irradiated with 24 GeV/c protons has been measured to be [2.6]:

$$\phi_{inv} = (18 \pm 0.6) N_{eff}(0) \quad (3.15)$$

The relation between the resistivity and  $N_{eff}$  as expressed by eq. 3.14 is not valid for irradiated diodes. Figure 3.7 shows  $\rho$  as a function of fluence in 1 MeV neutron irradiated diodes [3.32]. The resistivity increases as expected until  $\phi_{inv}$ , but for further fluence,  $\rho$  decreases with a

slower rate than the  $N_{eff}$  increase by a factor larger than 50. This indicates that a parameter associated to the material in thermal equilibrium ( $\rho$ ) and a parameter correlated to the material under reverse bias condition (depletion regime) cannot be correlated as expected from the theory of non-irradiated semiconductors.

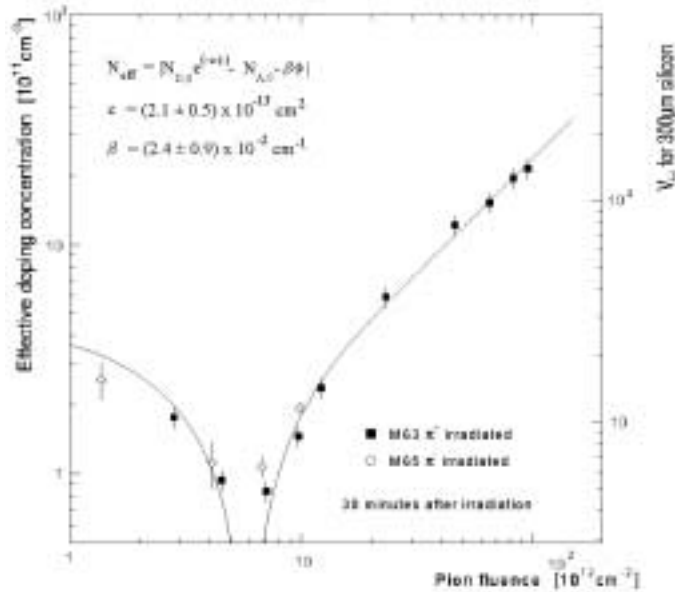


Fig. 3.6  $N_{eff}(V_{FD})$  as a function of pion fluence [3.28].

After inversion, a simple model describes the silicon detector as a p-type diode, which junction develops from the  $n^+$  rear layer. However, this model is inadequate to describe some behaviour of inverted detectors, as it will be discussed in Chapter 7.

$N_{eff}$  also exhibits a dependence on the time after irradiation. Figure 3.8 shows an example of  $V_{FD} (\propto N_{eff})$  as a function of time after irradiation for an inverted n-type detector.  $N_{eff}$  is found to decrease during  $\approx 10$  days at room temperature. After this *beneficial* annealing,  $N_{eff}$  starts to increase again. This increase takes place over many years at room temperature up to an apparent saturation. This second phase of the  $N_{eff}$  dependence on the time after irradiation is called *reverse annealing*. The reverse annealing data (for  $t > 10$  days) are well fitted by the form [3.28]:

$$N_Y(\phi, t, T) = N_{C0}(\phi) + N_{Y\infty}(\phi) \left[ 1 - (1 + N_{Y\infty}(\phi) k_Y(T) t)^{-1} \right] \quad (3.14)$$

where  $N_{Co}(\phi)$  is the stable damage component,  $N_{Y\infty}(\phi)$  is the saturation value at the end of the process and  $k_Y(T)$  is the reverse annealing rate constant.

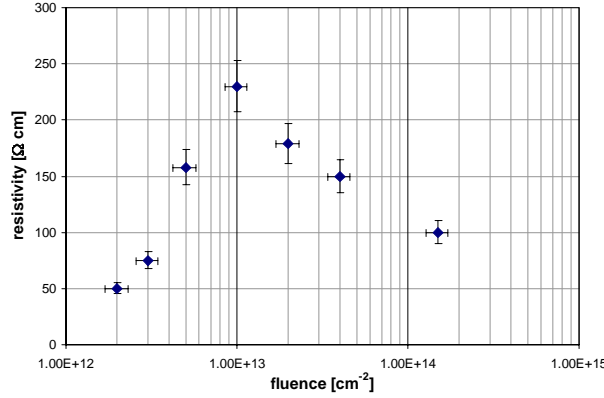


Fig. 3.7 Resistivity as a function of fluence (1 MeV neutrons) [3.32].

The amplitude of the reverse annealing can be expressed as a function of the fluence as following:

$$N_{Y\infty}(\phi) = g_Y \phi \quad (3.15)$$

In this parameterisation, the stable damage component and the final damage are found to be proportional to the accumulated fluence. Temperature cooling can significantly slow down the rates of both, beneficial and reverse the annealing, but it does not influence their final values. Inversely, it is possible to accelerate these processes by controlled temperature steps. Actually, the dependence of the rate constant  $k_Y(T)$  on the temperature  $T$  has been determined from anneals at various temperatures and found to follow an Arrhenius relation [3.28]:

$$k_Y(T) = k_0 \exp\left(-\frac{E_A}{k_B T}\right) \quad (3.16)$$

where  $k_0 = 520 \text{ cm}^3 \text{ s}^{-1}$  and  $E_A = (1.31 \pm 0.04) \text{ eV}$  [3.18]. Equation (3.16) is used to calculate the room temperature (20°C) equivalent annealing time.

This reverse annealing parameterisation seems to imply a second order process. If the irradiation produces two electrically inactive defects,  $X_1$  and  $X_2$ , in almost equal concentrations ( $N_{X1} \approx N_{X2} \approx N_X$ ), they can combine with each other to form electrically active acceptor states during the reverse annealing. If for example  $X_1 \equiv X_2$  the rate equation is

$$dN_X = -k_Y N_X^2 dt \quad (3.17)$$

which leads to the equation 3.14 with  $N_{Y\infty}(\phi)$  equal to the total concentration of the defect ( $N_X$ ).

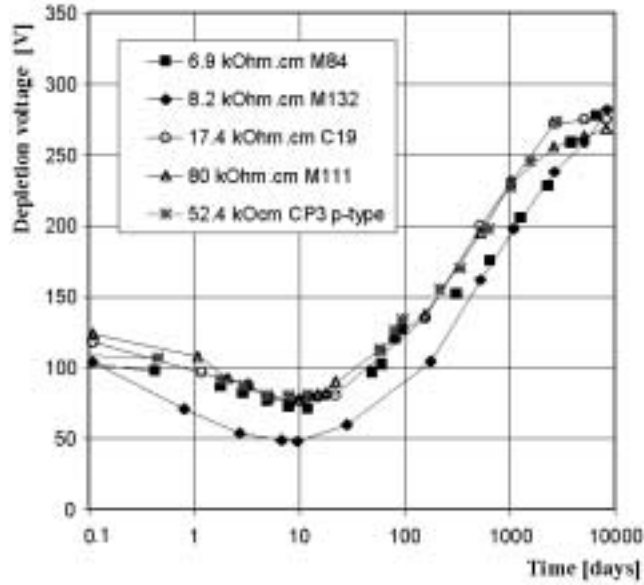


Fig.3.8 Depletion voltage (normalised to 300  $\mu\text{m}$  thickness) versus time after irradiation at room temperature for various high resistivity silicon detectors [2.6].

Actually, this situation seems unlikely. It has been evidenced [2.5, 3.29] that the reverse rate constant,  $k_Y$ , exhibits a  $1/\phi$  dependence. According to eq. 3.16,  $k_Y$  depends only on the temperature. This suggests that the reverse annealing is more likely caused by the composition of essentially first order processes [3.30] and eq. 3.14 represents a suitable parameterisation which minimises the number of parameters. Another good fit to the experimental data can be obtained by the sum of exponential term as it follows:

$$N_Y(\phi, t, T) = \sum_i N_y^i(\phi) \exp(-k_y^i t) \quad (3.18)$$

where  $N_y^i(\phi)$  is the contribution of the term  $i$ , with a rate constant  $k_y^i$ . Every term  $i$  of 3.18 accounts for a first order rate equation of the type:

$$\frac{dN_Y^i}{dx} = -k_Y^i N_Y^i \quad (3.19)$$

In this case the rate constant depends on the fluence, as can be seen by substituting eq. 3.15 in 3.19. However, the use of eq. 3.18 to fit the experimental data would require a too large number of parameters. Even if the sum is limited to two terms, which means that two dominant defects are involved into the process, the four fit parameters are correlated and they cannot be determined unambiguously. Therefore, fitting the experimental data with a sum of first order terms cannot help to clarify the reverse annealing mechanism, by providing the actual reaction rates.

Finally, even if the physical interpretation of the reverse annealing involves a composition of a few firsts order processes, the fit to the experimental data using eq. 3.14 is suitable, and it will be used in this work to compare the annealing behaviours of diodes made of different silicon materials.

### 3.2.3 Charge collection efficiency

The radiation-induced defects introduce deep levels in the silicon band gap, which act as traps for electrons and holes created by an ionising particle. The trapped charge can be successively released because of thermal excitation. This effect increases the charge collection time. When the detrapping (which is normally longer than the trapping time) is longer than the timescale of the measurement, an incomplete charge collection is performed.

The trapping effect results in an exponential decay of the number of the initially created pairs according to:

$$N_{e,h}(t) = N_0 \exp(-t/\tau_{tr,e,h}) \quad (3.20)$$

where  $\tau_{tr,e,h}$  is the carrier lifetime of electrons or holes. As long as the collection time is much lower than  $\tau_{tr,e,h}$  and the measurement time is longer than the collection time, the number of collected pairs is  $\approx N_0$ . When these times become comparable, the reduction of the collected charge due to the trapping starts to be effective. Further radiation increases the number of the trapping centres, reducing the trapping lifetime. The subsequent charge collection inefficiency, together with the increase of the noise, results in a worse signal to noise ratio in irradiated detectors, which finally could lead to the inability of detectors to discriminate the signal from the noise. Figure 3.9 shows the reduction of the charge collection efficiency as a function of 24 GeV/c proton fluence as measured in [3.20].

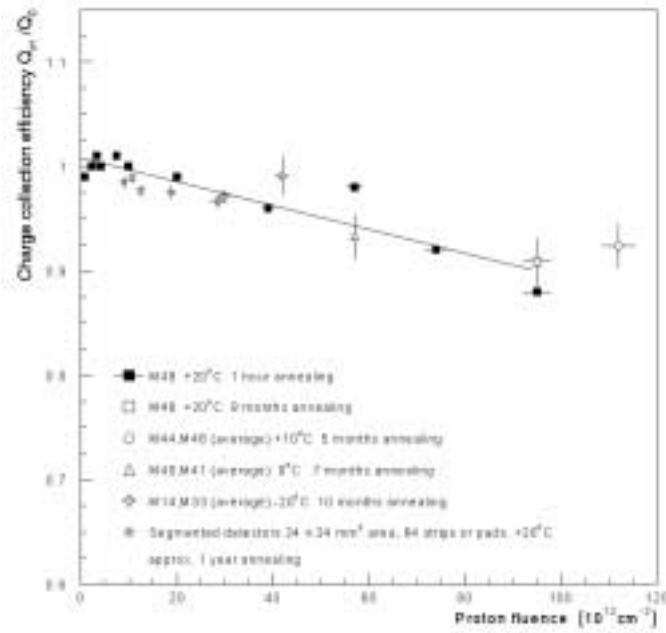


Fig. 3.9 Charge collection efficiency as a function of 24 GeV/c proton fluence [3.20].

### Effect on LHC detectors

The changes induced by the radiation degrade the characteristics of silicon detectors, which will eventually fail after heavy fluences. The detailed damage projection and operational scenario of the silicon detectors for the LHC experiment is beyond of the purposes of this thesis. However, a short description of the consequences of the damage on long-term operation of the detectors in a harsh radiation environment is sketched below.

The detector leakage current affects the electronic noise and the overall power consumption of the system. Design solution for the detector and the electronic read-out (detector capacitance, fast electronic shaping times...) can limit the influence of the shot noise. Moreover, the strong dependence of the leakage current on the temperature suggests operating the detectors at low temperature. Even a relatively modest cooling (from 20 to 5°C) can reduce the leakage currents by a factor  $\approx 4$ . This solution is very efficient for the leakage current and the excessive noise occupancy.

$N_{eff}$  changes are a serious problem for long time operations. For high resistivity detectors the expected value of  $N_{eff}$  after inversion is roughly equal to  $\beta\phi$  and  $\phi_{inv}$  is around  $1-2 \cdot 10^{13} \text{ cm}^{-2}$ . This represents only a small fraction of the fluence in the inner cavity of LHC detectors. The

value of  $N_{eff}$  after the fluence of  $1 \cdot 10^{14} \text{ cm}^{-2}$  1 MeV neutron is  $\approx 2.5\text{-}3 \cdot 10^{12} \text{ cm}^{-3}$ . The full depletion voltage for 300  $\mu\text{m}$  thick diodes with such a  $N_{eff}$  is  $\approx 200 \text{ V}$ , to which it is necessary to add 30-50V to operate in the overdepleted regime. This value of bias is dangerously high and close to expected breakdown voltages. The use of low resistivity silicon can push further  $\phi_{inv}$  and allows lower voltage than high resistivity detectors in order to achieve depletion after heavy irradiation. To this purpose, the detectors must be designed to operate up to 200-300 volts to achieve full depletion after irradiation. These values are without taking into account the annealing. This is influenced by the temperature, which can accelerate or slow down the beneficial and reverse annealing rates. Figure 3.10 shows the  $V_{FD}$  changes for detector irradiated between  $-20^\circ\text{C}$  and  $+20^\circ\text{C}$  [3.20].

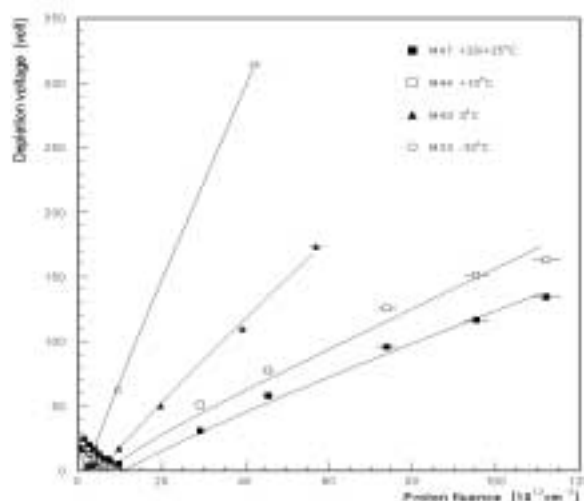


Fig. 3.10  $V_{FD}$  changes as a function of 24 GeV/c proton fluence for detector irradiated at various temperatures [3.20].

The low temperature irradiation results in higher  $V_{FD}$  immediately after irradiation because of the slowing down of the beneficial annealing that takes place during the irradiation. The reverse annealing is also slow down. The operation time in the bottom part of the annealing curve of  $N_{eff}$  ( $V_{FD}$ ), which is between 10 to 90 days at room temperature, is longer than 1 year at  $-20^\circ\text{C}$ . At very low temperature (liquid nitrogen) the behaviours of irradiated silicon detectors are completely different, due to the freezing of the deep traps.

Several predictions for the operation of silicon detectors after heavy irradiation have been

proposed by various workers [2.5, 3.19]. In the proposed scenarios, the operation at low temperature ( $\leq 0^\circ\text{C}$ ) is imperative for the survival of the detectors after heavy irradiation. The most likely failure mode will be the loss of the sensitive volume due to the excessive increase of  $V_{FD}$  ( $V_{FD} \leq V_{BD}$ ), leading to an underdepleted operation regime and subsequently to an insufficient S/N ratio.

These predictions have been obtained using the damage parameters available for standard silicon. The research of a material with  $\alpha$  and  $\beta$  lower than those of the standard silicon is still in progress.